

RYTSI: The Rochester Institute of Technology–Yale Tip-Tilt Speckle Imager

R. D. MEYER^{1,2}

Chester F. Carlson Center for Imaging Science, Rochester Institute of Technology, 54 Lomb Memorial Drive, Rochester, NY 14623-5604; rdmpci@cis.rit.edu

E. P. HORCH^{1,3}

Department of Physics, University of Massachusetts at Dartmouth, 285 Old Westport Road, North Dartmouth, MA 02747-2300; ehorch@umassd.edu

Z. NINKOV

Chester F. Carlson Center for Imaging Science, Rochester Institute of Technology, 54 Lomb Memorial Drive, Rochester, NY 14623-5604; zxnpci@cis.rit.edu

W. F. VAN ALTENA

Department of Astronomy, Yale University, P.O. Box 208101, New Haven, CT 06520-8101; vanalten@astro.yale.edu

AND

C. A. ROTHKOPF^{1,3}

Department of Brain and Cognitive Sciences, University of Rochester, Meliora Hall, Box 270268, Rochester, NY 14627-0268; crothkopf@bcs.rochester.edu

Received 2005 June 27; accepted 2005 September 18; published 2005 December 30

ABSTRACT. We have constructed a new speckle imaging system that collects a large number of speckle patterns on the detector area of a large-format CCD. The system is called the RIT-Yale Tip-tilt Speckle Imager (RYTSI) because it uses two galvanometric scanning mirrors to tip and tilt each speckle pattern to a different location on the CCD chip. It therefore solves the bandwidth problem of using CCDs in speckle imaging in a unique way: the mirrors direct speckle patterns across the chip with millisecond accuracy, and the CCD is read out only when the chip is filled with patterns. The instrument was designed to accommodate a variety of detector formats, readout systems, and telescope plate scales; it was initially used at the WIYN Observatory in conjunction with an RIT (Rochester Institute of Technology) 2048² CCD. We present the design of the instrument and a sample of first results, which indicate that the instrument can be expected to recover, with high precision, both astrometric and photometric information for binary and multiple stars.

1. INTRODUCTION

If a star's mass, surface temperature, luminosity, and metallicity are all known with high precision, only a small subset of all possible stellar models will agree with all four parameters simultaneously. If this combination of four parameters is likewise known for a large number of stars, this could potentially establish substantial constraints on astrophysics, such as the ranges of allowed mixing lengths and helium abundances. The only direct way to determine a star's mass is through observations of its gravitational influence on a companion; a precise measure of the mass requires a similarly massive companion. Thus, one must observe binary systems to measure stellar

masses directly. It then remains to measure the temperature, luminosity, and metallicity of the individual components of many such systems.

The surface temperature and luminosity can be deduced from photometric observations, but precise photometry requires that the components be clearly resolved. Most binary stars that are likely to have precise mass measurements have separations smaller than 1", the width of the typical seeing disk, which means their photometric study requires either high-resolution ground-based techniques or space-based observatories. The *Hubble Space Telescope* can resolve subarcsecond binaries, but its heavy demand and limited mission lifetime preclude the substantial binary star surveys required to meaningfully address astrophysics. *Hipparcos* surveyed many nearby binary systems and provided reliable photometric measurements for the systems it could resolve, but because it had only one bandpass, no component colors were measured.

Furthermore, these satellites have not reached the smallest binary star separations achievable by ground-based techniques; one such technique, speckle interferometry, in principle can reach the diffraction limit, or $\sim 0''.017$ at 5500 Å for an 8 m telescope.

¹ Visiting Astronomer, Kitt Peak National Observatory, National Optical Astronomy Observatory, which is operated by the Association of Universities for Research in Astronomy, Inc., under cooperative agreement with the National Science Foundation.

² Current address: TripAdvisor, Inc., 464 Hillside Avenue, Suite 304, Needham, MA 02494; meyer@tripadvisor.com.

³ Formerly of the Center for Imaging Science, Rochester Institute of Technology.

Speckle interferometry has been the method of choice for large-scale binary star surveys. It has yielded thousands of excellent angular separations and position angles (Mason et al. 2004; Horch et al. 2002, to name two of many examples). However, the bulk of speckle observations have been performed with ICCDs (intensified CCDs), which have proved difficult to calibrate for differential photometry, due to the strong nonlinearity of that type of detector, although some groups have tried (Prieur et al. 2003; Roberts 1998). Some investigators (e.g., ten Brummelaar et al. 2000; Turner et al. 2001) saw in adaptive optics a possible answer to the long-standing differential photometry problem, but adaptive optics does not yet enjoy the resolution achieved by speckle interferometry; at visible wavelengths, it has not reached the diffraction limit of large telescopes. More importantly, adaptive optics has not yet proven to be a large-scale survey technique. Some progress was made with the fork algorithm by Bagnuolo & Sowell (1988), but this has been applied only to extremely bright sources, such as Capella. Long-baseline optical interferometry holds great promise (Hummel et al. 1998), but is also currently limited to very bright objects. Thus, to conduct an extensive binary star survey that delivers high-quality photometric as well as astrometric measurements, it bears reinvestigating speckle interferometry to determine if a means presents itself to eliminate the calibration issues inherent in ICCDs.

To this end, we have simply substituted a CCD for the ICCD. The behavior of CCDs is well understood, and they are nearly linear devices. Others have applied CCDs to speckle interferometry (Klückers et al. 1997; Zadnik 1993), but they have not sustained efforts in this area, particularly with regard to the acquisition of accurate differential photometry.

Our group's first use of CCD detectors involved sequences of "speckle strips." This technique begins by laying down a speckle pattern on one small region of the CCD. The CCD is then rapidly shifted upwards in parallel by the number of rows corresponding to one speckle pattern, typically ~ 100 rows. A second speckle pattern is laid down on the CCD region where the first pattern had been; thus, the second pattern is imaged directly below the first pattern. By repeating this process, a strip of patterns, much like a motion picture film, is formed on the CCD from top to bottom. When the topmost pattern is shifted past the top edge of the CCD, it is clocked through the serial register and sent to the control computer for storage. Horch et al. (1997) describe the method in greater detail. The speckle-strip method requires a CCD with specialized electronics, capable of being clocked with a particular timing sequence; our group therefore always used an RIT (Rochester Institute of Technology) camera featuring a 2048^2 Kodak KAF-4200 CCD with this capability.

In 1998, three of us (Horch et al. 1998) proposed a second-generation CCD-based speckle instrument that would take advantage of the large format available in today's detectors to increase the observing efficiency. As illustrated in Figure 1, this concept, which became known as the RIT-Yale Tip-tilt

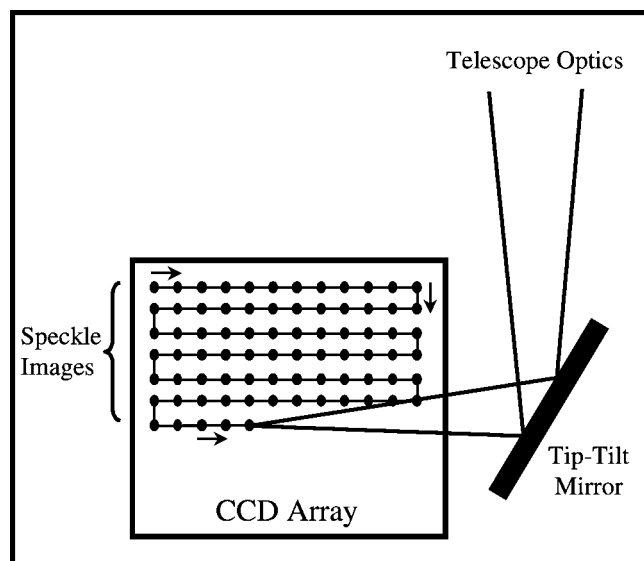


FIG. 1.—Diagram of RYTSI. A speckle pattern, the highly magnified short-exposure image of a telescope target, comes to a focus on a small location on a large CCD. By rotating the two orthogonal mirrors in the tip-tilt system, this pattern can be directed to any location on the CCD. Here, the mirrors start at the upper left corner of the CCD, they hold there for a fraction of a second while a speckle pattern accumulates, and then they quickly move to the right, where a second pattern is imaged. This sequence continues until the top rows of the CCD are filled, and then the mirrors step down to a new set of rows, ultimately filling the CCD, after which the full frame is read out of the CCD and archived. Typically, the speckle patterns are laid in a serpentine fashion, as depicted here.

Speckle Imager (RYTSI), incorporated a tip-tilt mirror system to direct the speckle pattern across the face of the CCD in both dimensions. In this manner, we would no longer require a CCD with specialized control electronics; standard full-frame CCD exposures would suffice. This would allow us to select a CCD based not on whether it allowed sophisticated timing, but rather on properties that are crucial for low-light applications, namely quantum efficiency and read noise. A detector with higher quantum efficiency and lower read noise, in combination with the enhanced observing efficiency made possible by spreading the patterns over a single large CCD frame, substantially improves the magnitude limit for a given exposure duration, and by reaching fainter targets, extends the science yield. For example, the low-mass end of the mass–luminosity relationship is poorly constrained, because so many of the M dwarf binaries at that end have simply been too faint to observe. From early observations made with RYTSI and the Mini-Mosaic camera at WIYN Observatory (Horch et al. 2004b), we estimate that that instrument combination can resolve, for the same exposure duration, systems with total magnitudes ~ 1.3 mag fainter than the 10th magnitude systems (Horch et al. 2002) that had been obtainable with our group's former instrumentation, vis-à-vis the RIT 2048^2 camera taking speckle strips. This magnitude limit should further improve with recent CCD technology, e.g.,

the Fairchild 486 CCD within a Spectral Instruments camera purchased by RIT in 2004.

The final form of RYTSI is sufficiently different from the concept envisioned in Horch et al. (1998) that we describe it in § 2 below. To utilize the data-reduction routines that were developed for the speckle-strip method, it is necessary to extract a speckle sequence from the two-dimensional array of speckle patterns that comprises a RYTSI CCD image; in § 3 we propose a technique to perform this conversion. In § 4 we present binary star image reconstructions and preliminary astrometric and photometric results from early RYTSI observations. Additional details regarding RYTSI can be found in Chapter 5 of Meyer (2002).

2. DESIGN

RYTSI is designed to mount directly onto the instrument plane of a variety of telescopes, and in turn to allow a variety of detectors to mount onto its back plane. As such, its main enclosure contains the optics that a speckle interferometry observation requires to manipulate the light in its passage from the telescope to the detector. These optical components address several categories: beam redirection, via the tip-tilt mirror system; wavelength selection, via a double filter wheel; time selection, via a shutter; and atmospheric dispersion correction, via a (planned) pair of Risley prisms. A pair of lenses provides a collimated beam for most of these components, and it magnifies the speckle pattern delivered by the telescope in order to approximately critically sample the image.

The optical components are all ultimately mounted to a 1/2 inch (12.7 mm) thick bottom plate; this “optical bench” and four 3/8 inch (9.5 mm) thick vertical walls provide a rigid enclosure to minimize flexure concerns. This light-tight enclosure and its optical mounts consist entirely of black anodized aluminum.

The top half of Figure 2 is a photograph of the interior of RYTSI; the diagram in the bottom half elucidates the essential features. Light enters the instrument through the front wall (*top*). A shutter here provides exposure control. The telescope’s focus is nominally 1.5 inches (3.81 cm) inside the front wall’s external face. To measure field distortion, a reticle is routinely placed at this focus. There is also room to mount a field stop here, if it becomes necessary to block light from nearby background objects.

The light next passes through the first of the pair of lenses. When RYTSI is mounted at the Nasmyth instrument port at WIYN, an $f = 60.0$ mm lens is used; in this case the reimaging lens has $f = 180.0$ mm. This has been the configuration for all observations discussed herein. For the Cassegrain port, the collimating lens has $f = 100.0$ mm, and the corresponding reimaging lens has $f = 160.0$ mm. All lenses are currently Melles Griot achromats with 30.0 mm diameters.

The light next encounters the first mirror, which has a flat, 25 mm diameter, $\lambda/10$ protected silver surface. It is oriented at 45° with respect to the incident collimated beam, and is

present so that the final beam, after reflecting off of the two tip-tilt mirrors, exits the instrument opposite the telescope.

The light beam next traverses an area reserved for future Risley prisms. This pair of Risley prisms would compensate for the elongation of the speckles due to differential atmospheric refraction. The Risley prism motors and electronics have been acquired but not installed, because WIYN’s Nasmyth instrument port has an internal atmospheric dispersion correction (ADC) unit. The elongation in the reconstructed images given in § 4, particularly in Figure 7 (which depicts the trinary BU 1295), is present probably because we did not engage the WIYN ADC at this early stage in our RYTSI observations.

Next, the light enters an assembly of two independently controllable filter wheels. Each wheel has positions for eight 1 inch (2.54 cm) diameter filters, providing as many as 14 filters if one position is kept clear on each wheel. Currently, the first wheel houses neutral density (ND) filters, while the second wheel houses a Johnson *V* filter and several intermediate-bandpass interferometric filters. We have measured the transmission curves of all of these filters at RIT, using an Acton SpectraPro 500 monochromator and a regulated Oriel 6337 light source. For the colored filters, we measured the transmission twice, with one side of the filter facing the lamp, and then the other side; the final curve is the average of these two measurements. Figure 3 presents these transmission curves, together with the quantum efficiency curve of the CCD used in the initial RYTSI observations. This is the same 2048² Kodak KAF-4200 CCD that was used in our group’s previous CCD speckle work (Horch et al. 2004a, and references therein; Horch et al. 2000).

Table 1 lists the colored filters’ bandpasses, as computed from both our transmission curve measurements and the curves supplied by the filters’ manufacturers. For the interference filters, the manufacturers’ curves differ from ours primarily by a translation in wavelength (~ 13 Å in the worst case), and to a lesser extent by a change in width (the bandpasses apparently broadened somewhat with time). We have previously seen a translation of filter transmission for other interference filters (Meyer 2002, p. 129). There are also some small differences in shape between the manufacturers’ curves and ours. These shape differences are probably negligible for all but the most exacting photometric calibrations. Nevertheless, these differences indicate that we should continue to measure the curves with the same technique in order to minimize filter transmissions as a source of concern in photometry derived from RYTSI.

The ND transmission curves agree very closely in shape with the curves provided by the manufacturer; however, the overall heights of the RIT measurements differ from the manufacturer’s, as if the transmission increased with time. The increase is greater with higher ND, ranging from $\sim 4.5\%$ for $ND = 0.3$ to $\sim 21\%$ for $ND = 2.0$.

Next in the optical path are the tip-tilt mirrors, which are two SS200 galvanometric scanning mirrors furnished by Laserworks of Santa Ana, California. Each is oriented at $\sim 45^\circ$

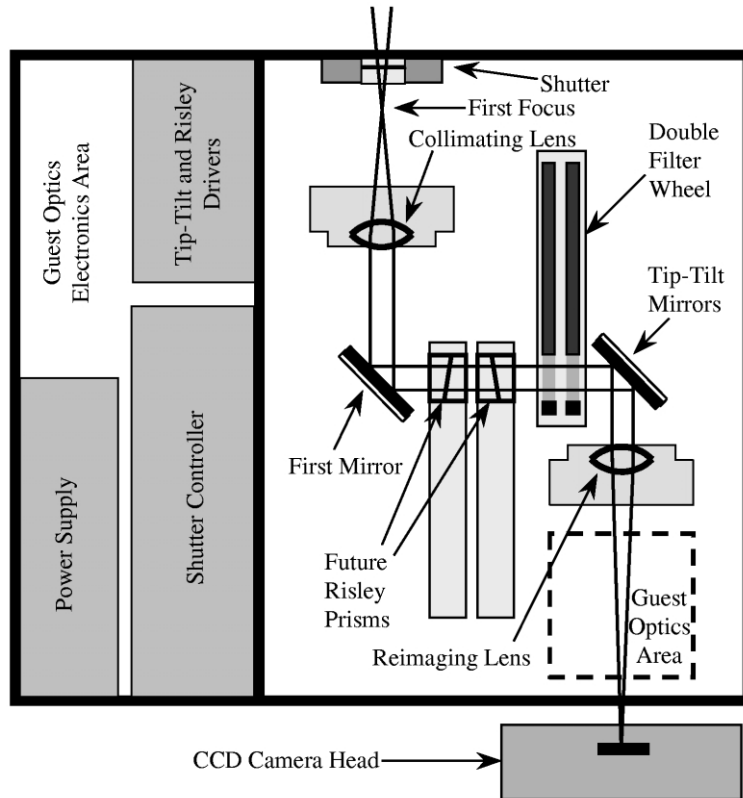
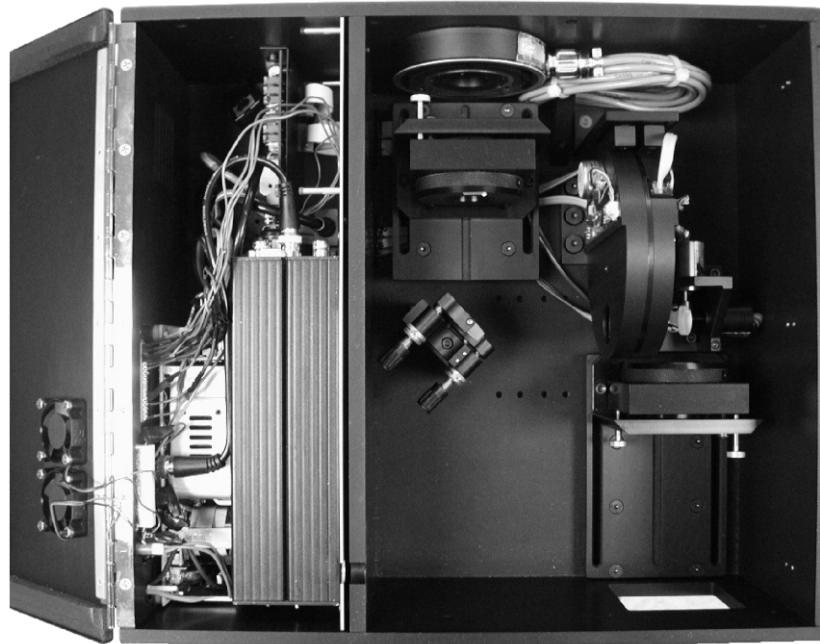


FIG. 2.—Photograph and diagram of the interior of RYTSI, reprinted with permission from Meyer (2002). See text for details.

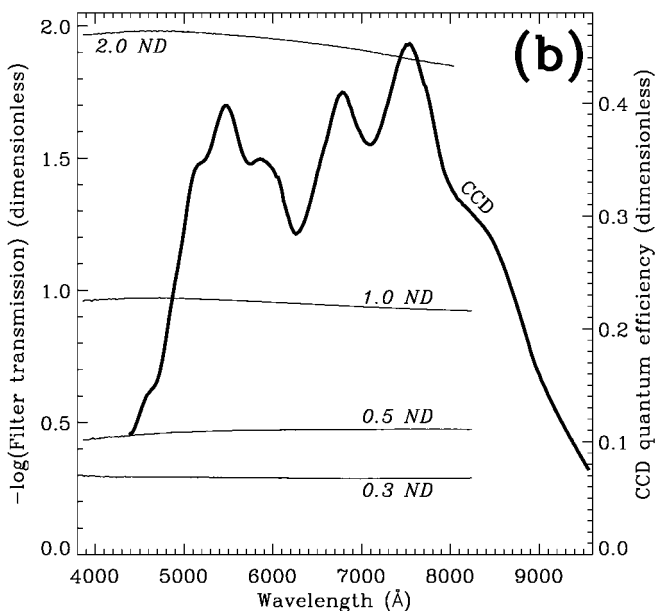
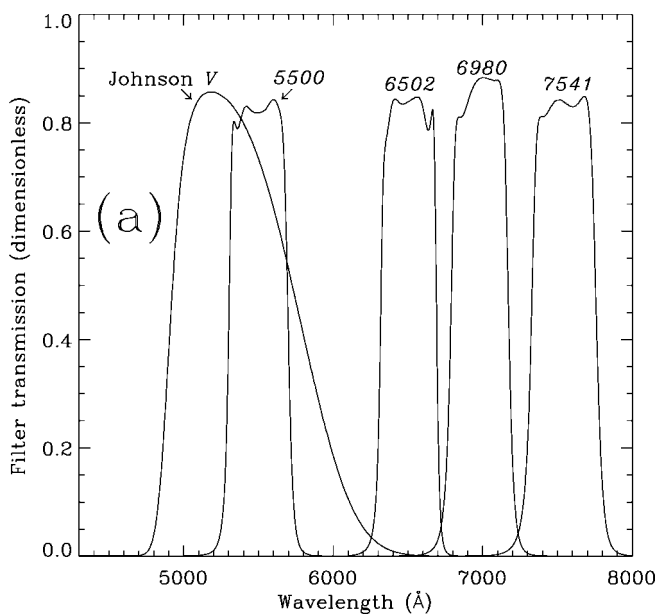


FIG. 3.—RYTSI filter transmissions and RIT CCD quantum efficiency (QE) curve. (a) RYTSI's colored filters, consisting of four intermediate-band interferometric filters and a Johnson V filter. (b) The QE curve for the RIT Kodak KAF-4200 CCD used in the initial RYTSI observations, overlaid on the transmissions (logarithmic scale) of RYTSI's neutral density filters. QE curve measured 2000 November 13; Table 1 lists filter measurement dates. All measurements conducted at RIT.

TABLE 1
RYTSI FILTER CHARACTERISTICS

Filter Name	Mean λ (\AA)	FWHM (\AA)	Date Measured
Measurements conducted at RIT:			
V	5387.4	875	2004 Feb 24
5500	5499.6	399	2004 Feb 23
6502	6502.5	376	2004 Feb 23
6980	6980.3	387	2004 Feb 24
7541	7541.2	437	2004 Feb 24
Manufacturer's transmission curves:			
V	5504.7	827	N/A ^a
5500	5512.2	391	2001 Mar 29
6502	6501.3	374	2001 Mar 06
6980	6989.1	382	2000 Jun 28
7541	7529.0	418	2000 Oct 18

^a Not available; values computed from curve from Straizys (1977, p. 84)

relative to the collimated beam and can be driven to 4096 digital steps. The closed-loop motor system exhibits consistent positioning performance, with some repeatable hysteresis that the control software easily corrects during observations.

The beam next enters the reimaging lens, which converges the beam as it passes through an area reserved for optional guest optics. The beam focuses on the detector, generally a CCD, which is mounted to the back wall of RYTSI.

Because telescopes have differing plate scales, and detectors have various pixel sizes and back focal distances, RYTSI must be able to accommodate a range of magnifications and focal positions. RYTSI is easily reconfigured by replacing the lens pair and moving the lens mounts along the optical axis on special tracks. Beam realignment is primarily accomplished by rotating the tip-tilt mirrors about their rotation axes, with finer scale adjustment performed with the pitch and yaw adjustment knobs on the first mirror. The lens pair mounts also contain pitch and yaw knobs, but in practice these remain fixed.

The tip-tilt motor driver electronics, shutter controller, and main instrument power supply are contained in a thermally isolated bay (see left third of Fig. 2). Most major onboard heat sources are confined to this electronics bay, with the exceptions being the tip-tilt mirror motors, the shutter itself, and the filter wheel driver circuits and motors.

RYTSI is controlled through an interface computer in the WIYN control room. A custom C++ program drives the tip-tilt mirrors through a National Instruments AT-AO-6 board. Software communicates with the filter wheels via the computer's parallel port. The shutter is generally triggered directly by the CCD camera, which, being an independent system by design, has its own control lines and software.

3. OBSERVATIONS AND DATA REDUCTION

After completing the instrument in Rochester, in 2001 June we brought it to the WIYN 3.5 m telescope at Kitt Peak for first observations. Since then, it has been successfully used on several occasions at WIYN. The results described in § 4 rep-

resent a brief selection from the first three runs: 2001 June–July, 2001 October, and 2002 April. In these runs, the RIT Kodak KAF-4200 CCD served as the detector. Seeing ranged from approximately $0''.6$ to somewhat over $1''$ during these three runs. The plate scale, as determined from telescope offsets, was $0''.028 \text{ pixel}^{-1}$.

The RYTSI data files were not flat-fielded when reduced for this paper. The instrument presents a highly vignetted field to the CCD camera; it was designed this way so that a star near the target usually would not produce significant signals on the CCD that could intermingle with the speckle patterns of the target. Therefore, for any one tip-tilt mirror position, only a relatively small portion of the CCD is fully illuminated; at WIYN, this unvignetted region is approximately elliptical, with axes of $\sim 14''$ and $\sim 10''$. The target star is nominally centered within this region and remains fixed relative to this region as the galvanometric mirrors tip and tilt this small field across the CCD.

We took a series of dome flats with the mirror voltages set at various positions; each voltage change placed the center of the unvignetted area over a different location on the CCD chip. If the flat-field illumination is a strong function of mirror position, this should manifest as structural variations of the unvignetted region among these dome flats. When we compared flats in which the unvignetted area was near the corners of the CCD to flats where it was nearly in the center of the array, we found no significant changes in the flat-field illumination. Furthermore, the unvignetted region itself showed a quite flat response, with little low-frequency variation; variations within the region were less than $\sim 1\%$. The RIT 2048^2 CCD chip also has a nearly flat response, with few cosmetic defects. We concluded that for the purpose of demonstrating the basic capabilities of the system, further attention to flat-fielding was unnecessary. The flat-fielding will be examined in more detail in the paper that presents the first substantial list of astrometric and photometric results with RYTSI.

In order to extract individual speckle patterns from a 2048×2048 full-frame CCD exposure, a four-step process is employed. First, a copy is made of the full-frame image, and this copy is spatially filtered. The filter function, being the difference between two Butterworth filters that differ slightly in width, is near zero everywhere except within an annulus in the frequency plane. The filtering is accomplished by multiplying the filter function by the Fourier transform of the full frame and then performing the inverse Fourier transformation; this is equivalent to convolving the image with the inverse transform of the Butterworth-difference filter. The objective is to retain in the image only features of a given size—in this case, the size of a typical speckle pattern. The patterns appear as smooth peaks in the filtered image.

Second, the filtered image is thresholded, setting pixels above a certain fraction of the maximum to 1, and below that same value to zero. The third step is to mark each connected region in the image, and for each one, compute the midpoint between the minimum and maximum values in x and y for

pixels in that region. Finally, a box that is 128×128 pixels in size is centered on the midpoint of each connected region, and subframes are extracted from the locations on the original full-frame image corresponding to each box. Figure 4 shows a typical CCD exposure with these 128×128 boxes overlaid. The 128×128 pixel subframes are then stacked together and written out in FITS format. The time ordering of the stack is inconsequential for the speckle analysis and is therefore not strictly enforced when assembling the stack.

Once speckle patterns have been extracted from a RYTSI exposure, calibrated, and then ordered into a sequence, they can be fed into the same data-reduction pipeline that was developed for the speckle-strip method. This pipeline is discussed in Horch et al. (1997); analyses of the resulting astrometric and photometric measurements, including comparisons with observations in the literature, can be found, for example, in Horch et al. (2002, 2004a). We have not yet performed the equivalent analyses on RYTSI observations, so we do not present results from this data pipeline here. Instead, the next section involves reconstructed images generated through the methodology outlined in Lohmann et al. (1983). This technique uses bispectral analysis to assemble the Fourier components of the diffraction-limited image. The astrometric and photometric quantities presented in § 4 are computed directly from these reconstructed images, and therefore should be treated as approximate.

4. INITIAL RESULTS

We show here results for two known binary stars, BU 151 (HIP 101769, WDS 20375+1436) and YR 2 (HIP 98055, WDS 19556+5226), and one known triple system, BU 1295AB and STF 566AB-C (HIP 21730, WDS 04400+5328). YR 2 has a modest magnitude difference, which is approximately 0.7 mag. This system is an interesting test case, because its separation, $\sim 0''.1$, is near the diffraction limit of WIYN, which is $0''.040$ at 5500 \AA . Because both of the components of BU 151 have evolved off of the main sequence (Meyer 2002, p. 181), its component temperatures and luminosities change more quickly with time, making that system an unusually strong constraint on astrophysics.

Figure 5a shows four speckle patterns of YR 2, extracted from a 2048×2048 CCD frame. These patterns clearly illustrate the classic “double speckle” appearance of a small-separation point source. Figure 5b contains the power spectrum made from 1024 individual speckle frames of the target. As expected, it has very high signal-to-noise ratio fringes running perpendicular to the vector separation on the image plane. A routine in our data-reduction pipeline fits a cosine-squared function to power spectra like this to derive the separation, position angle, and magnitude difference at the epoch of observation. The fringes indicate data products of typical quality for a target of this type.

In Figures 6, 7, and 8, we present diffraction-limited image reconstructions for the three stars mentioned above. In the case

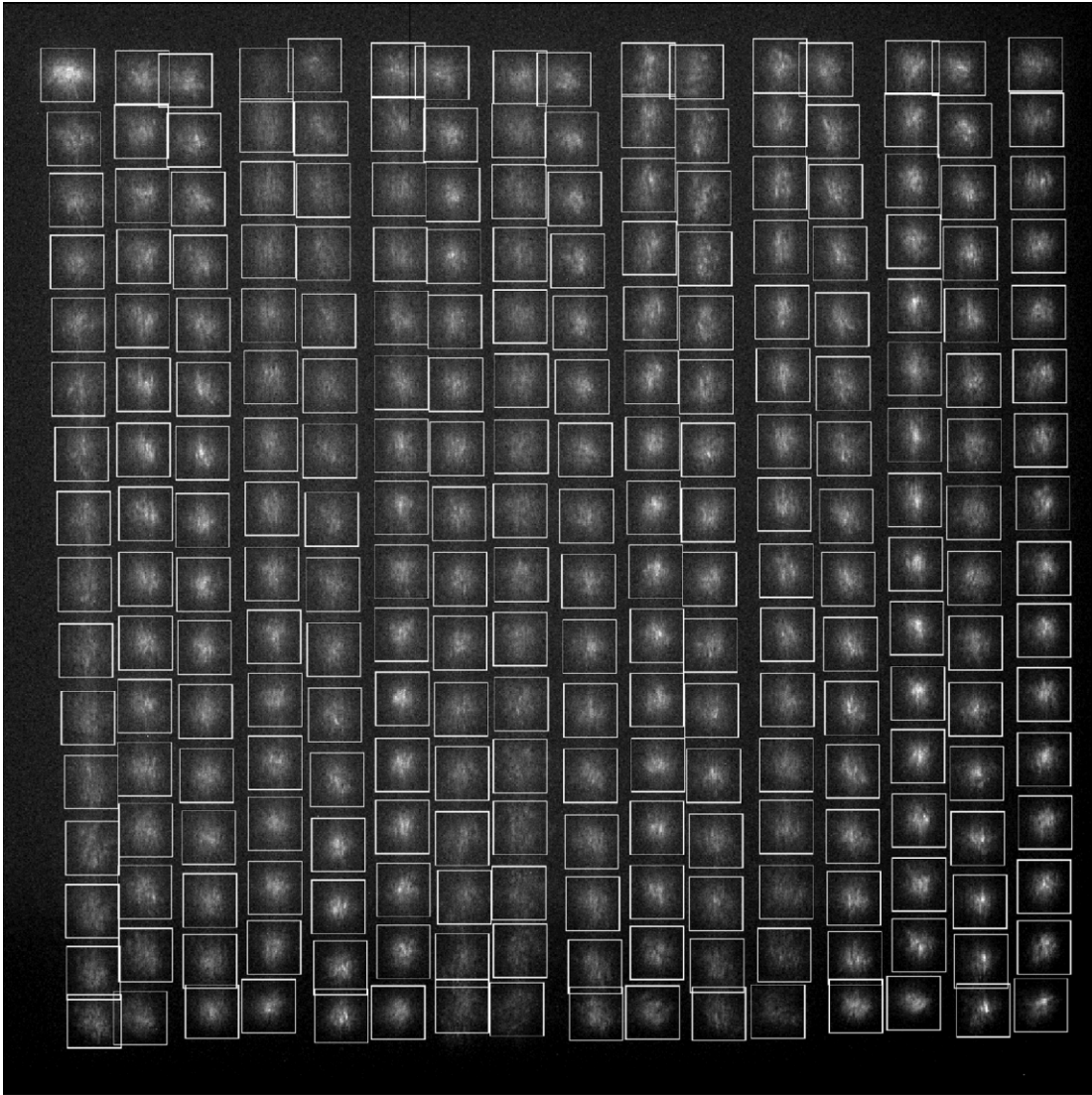


FIG. 4.—Full-frame CCD exposure with RYTSI, with subframes depicted. The underlying image is the result of a 16×16 serpentine, as exemplified in Fig. 1. The boxes denote where the algorithm that is described in § 3 detected each speckle pattern and defined each subframe. The subframes are then ordered into a one-dimensional speckle sequence.

of Figure 6, which is the reconstructed image of YR 2, the two stars are clearly resolved, with the secondary at a position angle of $\sim 80^\circ$, but there is a peak at the 5% level 180° away from the location of the secondary star. The phase-reconstruction program that we use starts from the so-called zero-phase assumption for the Fourier transform of the reconstructed image, and then iterates to find the phase map most consistent with the bispectral subplanes being analyzed. This sometimes results in a “ghost peak” in the reconstructed image, especially for binaries with modest magnitude differences, where the phase information in the bispectrum is not very different from the zero-phase case. Figures 7 and 8 show high-quality image re-

constructions of BU 1295 and BU 151, respectively, with the highest noise peaks at the 2%–3% level.

Table 2 lists astrometric and photometric results from these and other images reconstructed from RYTSI observations of these three targets. In particular, there are three observations listed for the triple system in each of two filters, and there are three observations listed for BU 151. Because we have not yet fully analyzed a large sample of data and do not yet have robust calibrations for the astrometry, these data should all be viewed as preliminary. For example, the data in Table 2 were derived by fitting two-dimensional Gaussian distributions to the reconstructed images, whereas the standard, well-tested data pipeline

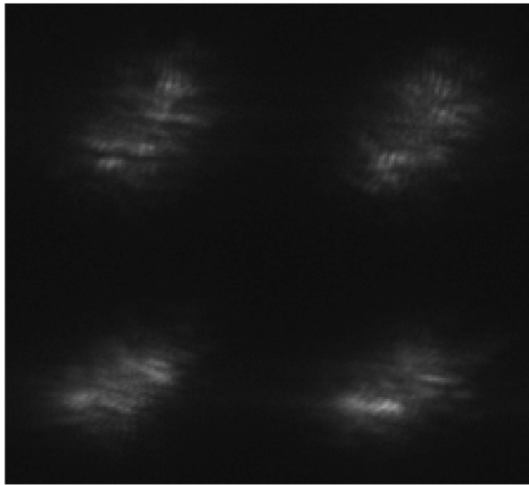


Fig 5a

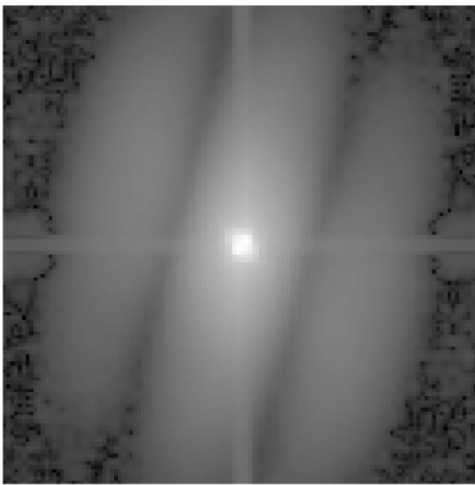


Fig. 5b

FIG. 5.—(a) Magnified portion, showing four adjacent speckle patterns, of a full-frame RYTSI exposure of YR 2, taken on 2001 June 29 with the 6980 filter. Roughly, north is toward the bottom and east is toward the right. Double speckles are obvious in each pattern, particularly in the top two patterns; they are aligned in a direction just north of east. (b) Preliminary power spectrum computed from all 1024 speckle patterns that encompass the 6980 observation of YR 2. Note that the fringes are oriented in the same direction as the double speckles in (a). The corresponding separation and position angle are $\rho = 0''.096$ and $\theta = 79^\circ 0$, which indicate that the system moved somewhat since a 1997 observation of YR 2, when $\rho = 0''.085$ and $\theta = 99^\circ 4$ had been measured. Images reprinted with permission from Meyer (2002, p. 206).

fits a cosine-squared function to the power spectra. Nonetheless, the level of internal consistency between different values of position angle and separation is very high. In addition, BU 151 and BU 1295AB have well-determined orbits (Alzner 1998; Hartkopf et al. 1996), and the separation and position angle

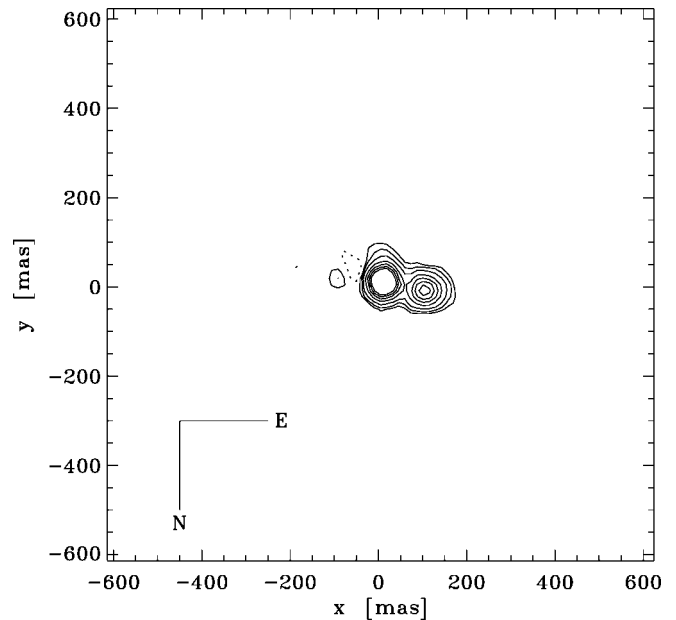


FIG. 6.—Reconstructed image from the 5500 observation of YR 2 (HIP 98055; see Table 2). Contour levels are drawn at $-0.025, 0.025, 0.05, 0.1, 0.2, 0.3, 0.4,$ and 0.5 of the image maximum, which is the peak of the primary star. The innermost contour on the primary is therefore indicative of the FWHM of the reconstructed image of a point source. The compass in the lower left depicts the image orientation.

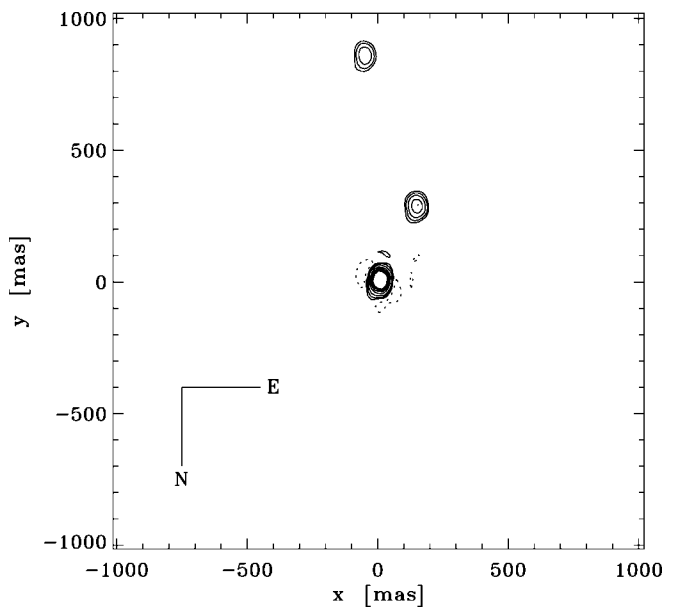


FIG. 7.—Same as in Fig. 6, but for one of the three 5500 observations of BU 1295 (HIP 21730).

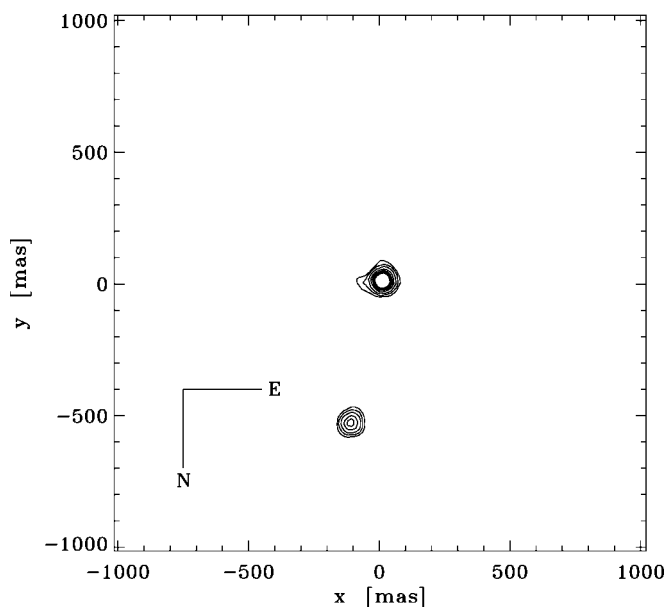


FIG. 8.—Same as in Fig. 6, but for the 6980 observation of BU 151 (HIP 101769).

values reported in Table 2 are consistent with the orbit ephemerides for the observation epochs in question, given our lack of precision at this point in the scale determination.

The magnitude differences listed in Table 2 also have a high degree of internal consistency, on the level of a few hundredths of a magnitude for observations of the same object taken in the same filter. Looking at the results for the triple system, this level of scatter is significantly smaller than the differences between the average values obtained in each filter; this indicates that we are seeing the intrinsic color difference between the components.

Perhaps the best way to assess the accuracy of RYTSI photometry would be to insert into the optical beam a calcite crystal and a linear polarizing filter that can rotate with respect to the crystal; the relative intensity between the two resulting images of a single star is a predictable function of the orientation of the polarizing filter (Barry et al. 1992). We have not yet obtained the crystal and filter, but it should be fairly straightforward to perform this test, given the ability of the instrument to accommodate such optics. In lieu of this experiment, photometric accuracy can be estimated by comparing the RYTSI differential measurements to magnitude differences provided by other sources. We intend to perform this comparison in detail prior to publication of the first substantial set of RYTSI photometry; however, we offer a simplistic comparison here that suggests that the RYTSI measurements are not grossly discrepant from other photometric techniques. Table 3 lists magnitude differences for the binary stars considered in the present paper, as derived from speckle strips taken with the RIT 2048² CCD; these were presented in Horch et al. (2004a). That paper demonstrated the consistency between its measurements and two other substantial contributions to binary star differential photometry, namely the *Hipparcos* catalog (ESA 1997) and the adaptive optics results of ten Brummelaar et al. (2000). Upon comparing entries in Tables 2 and 3 for the same star at similar bandpasses, the accuracy of the RYTSI magnitude differences does not appear to be significantly worse than the level of internal precision. While it entails a small study, Table 2 is evidence that RYTSI will be able to determine the magnitudes and colors of individual components of close binary stars.

5. CONCLUSION

We have presented the design of a new speckle imaging system that was built in Rochester, New York, and is now in

TABLE 2
PRELIMINARY RESULTS FROM BINARY STAR IMAGES RECONSTRUCTED FROM
RYTSI OBSERVATIONS

HIP Number	Other Designations	Besselian Year	ρ (arcsec)	θ (deg)	Δm (mag)	Filter
98055	YR 2	2001.493	0.095	78.3	0.67	5500
	WDS 19556+5226	2001.493	0.096	79.0	0.68	6980
21730 (AB)	BU 1295AB WDS 04400+5328	2001.758	0.312	153.1	1.37	5500
		2001.758	0.313	153.5	1.35	5500
		2001.758	0.313	153.2	1.31	5500
		2001.758	0.311	153.3	1.24	6980
		2001.758	0.312	153.3	1.27	6980
21730 (AB-C)	STF 566AB-C WDS 04400+5328	2001.758	0.311	153.5	1.29	6980
		2001.758	0.853	183.9	2.04	5500
		2001.758	0.853	184.0	2.09	5500
101769	BU 151 WDS 20375+1436	2001.758	0.856	184.0	1.95	5500
		2001.758	0.851	183.8	1.81	6980
		2001.758	0.853	183.9	1.82	6980
		2001.758	0.855	183.9	1.85	6980
		2002.323	0.578	349.4	1.17	6502
		2001.495	0.553	347.4	1.11	6980

TABLE 3
DIFFERENTIAL PHOTOMETRY FROM HORCH ET AL. (2004a)
FOR THE STARS IN TABLE 2

HIP Number	Besselian Year	Δm (mag)	Filter $\lambda \pm \Delta\lambda$ (nm)
21730	2000.7651	1.18	503 \pm 40
(AB)	1997.8299	1.20	648 \pm 41
	1998.9274	1.08	648 \pm 41
	1999.8859	1.14	701 \pm 12
21730	2000.7651	2.06	503 \pm 40
(AB-C)	1997.8299	1.76	648 \pm 41
	1998.9274	1.65	648 \pm 41
	1999.8859	1.60	701 \pm 12
101769	2000.7615	1.11	503 \pm 40
	2000.7671	0.99	503 \pm 40
	1997.6134	1.03	551 \pm 10
	1999.6394	1.13	551 \pm 10
	2000.6168	1.00	551 \pm 10
	1999.6394	1.18	648 \pm 41
	2000.6168	1.07	648 \pm 41
	2000.7615	1.21	648 \pm 41
	2000.7671	1.06	648 \pm 41
	1997.5177	0.99	701 \pm 12
	1997.5177	1.04	701 \pm 12
	1997.6134	1.08	701 \pm 12
	1997.6159	1.11	701 \pm 12
	1999.6394	1.18	701 \pm 12
	2000.6168	1.04	701 \pm 12

use at the WIYN 3.5 m telescope at Kitt Peak National Observatory. This unique system takes advantage of the entire area of a large-format CCD camera to collect a large number of speckle patterns before full-frame readout, and it is compatible with a variety of such cameras. The first results indicate

that the instrument is capable of high-quality speckle imaging. The technology employed is inexpensive and could easily be replicated at other observatories that already have large-format CCDs for more conventional astronomical imaging applications. As of this writing, RYTSI has been used at WIYN on several successful runs, and the initial results presented here appear typical of the subsequent runs; the quality of these results also appears to match the expectations set by previous CCD-based speckle imaging at WIYN.

The main scientific advantage of this approach is that it permits the retrieval of accurate differential photometry down to the diffraction limit of the telescope, in addition to the high-precision astrometry for which speckle imaging is well known. This suggests that RYTSI could play an important role in determining the component temperatures and luminosities of many binary systems that have mass measures of interest to stellar astrophysics, and in the empirical mass–luminosity relationship.

The authors gladly thank Steven Uhl and Gunnar Richardson of Modelmax Corp., East Rochester, New York, for their superb machining of the main instrument, and the staff of Kitt Peak, particularly Charles Corson, Hillary Mathis, Eugene McDougall, George Will, and Doug Williams, for their help in interfacing RYTSI with the WIYN telescope and for providing their expertise during observing. The authors also thank the anonymous referee for beneficial comments. The construction of the instrument was funded through NSF grant AST-9731165, and funds for the publication of this paper were made available by the College of Engineering at the University of Massachusetts, Dartmouth.

REFERENCES

- Alzner, A. 1998, *A&AS*, 132, 253
 Bagnuolo Jr., W. G., & Sowell, J. R. 1988, *AJ*, 96, 1056
 Barry, D. J., Bagnuolo, W. G., Mason, B. D., McAlister, H. A., & Turner, N. H. 1992, in *ASP Conf. Ser. 32, Complementary Approaches to Double and Multiple Star Research*, ed. H. A. McAlister & W. I. Hartkopf (San Francisco: ASP), 537
 ESA. 1997, *The Hipparcos and Tycho Catalogues* (ESA SP-1200; Noordwijk: ESA)
 Hartkopf, W. I., Mason, B. D., & McAlister, H. A. 1996, *AJ*, 111, 370
 Horch, E. P., Franz, O. G., & Ninkov, Z. 2000, *AJ*, 120, 2638
 Horch, E. P., Meyer, R. D., & van Altena, W. F. 2004a, *AJ*, 127, 1727
 Horch, E. P., Ninkov, Z., & Slawson, R. W. 1997, *AJ*, 114, 2117
 Horch, E. P., Ninkov, Z., & van Altena, W. F. 1998, *Proc. SPIE*, 3355, 777
 Horch, E. P., Riedel, H., van Altena, W. F., Meyer, R. D., & Corson, C. 2004b, *BAAS*, 36, 787
 Horch, E. P., Robinson, S. E., Meyer, R. D., van Altena, W. F., Ninkov, Z., & Piterman, A. 2002, *AJ*, 123, 3442
 Hummel, C. A., Mozurkewich, D., Armstrong, J. T., Hajian, A. R., Elias II, N. M., & Hutter, D. J. 1998, *AJ*, 116, 2536
 Klückers, V. A., Edmunds, M. G., Morris, R. H., & Wooder, N. 1997, *MNRAS*, 284, 711
 Lohmann, A. W., Weigelt, G., & Wirtitzer, B. 1983, *Appl. Opt.*, 22, 4028
 Mason, B. D., Hartkopf, W. I., Wycoff, G. L., Rafferty, T. J., Urban, S. E., & Flagg, L. 2004, *AJ*, 128, 3012
 Meyer, R. D. 2002, Ph.D. thesis, Yale Univ.
 Prieur, J.-L., Carquillat, J.-M., Ginestet, N., Koechlin, L., Lannes, A., Anterrieu, E., Roques, S., Aristidi, E., & Scardia, M. 2003, *ApJS*, 144, 263
 Roberts, L. C., Jr. 1998, Ph.D. thesis, Georgia State Univ.
 Straižys, V. 1977, *Multicolor Stellar Photometry* (Vilnius: Mokslas)
 ten Brummelaar, T., Mason, B. D., McAlister, H. A., Roberts, Jr., L. C., Turner, N. H., Hartkopf, W. I., & Bagnuolo, Jr., W. G. 2000, *AJ*, 119, 2403
 Turner, N. H., ten Brummelaar, T. A., McAlister, H. A., Mason, B. D., Hartkopf, W. I., & Roberts, Jr., L. C. 2001, *AJ*, 121, 3254
 Zadnik, J. A. 1993, Ph.D. thesis, Georgia Inst. Tech.